EXPERT REVIEWS

Anterior-segment imaging for assessment of glaucoma

Expert Rev. Ophthalmol. 5(1), 59–74 (2010)

Roxana Ursea and Ronald H Silverman†

†*Author for correspondence*
Department of Ophthalmology, Weill Cornell Medical College, 1300 York Avenue, Room LC303, NY 10065, USA
Tel.: +1 212 746 6106
Fax: +1 212 746 8101
ros2012@med.cornell.edu

This article summarizes the physics, technology and clinical application of ultrasound biomicroscopy (UBM) and optical coherence tomography (OCT) for assessment of the anterior segment in glaucoma. UBM systems use frequencies ranging from approximately 35 to 80 MHz, as compared with typical 10-MHz systems used for general-purpose ophthalmic imaging. OCT systems use low-coherence, near-infrared light to provide detailed images of anterior segment structures at resolutions exceeding that of UBM. Both technologies allow visualization of the iridocorneal angle and, thus, can contribute to the diagnosis and management of glaucoma. OCT systems are advantageous, being noncontact proceedures and providing finer resolution than UBM, but UBM systems are superior for the visualization of retroiridal structures, including the ciliary body, posterior chamber and zonules, which can provide crucial diagnostic information for the assessment of glaucoma.

Keywords: anterior segment • eye • glaucoma • imaging • optical coherence tomography • ultrasound biomicroscopy

MedscapeCME™ **Medscape: Continuing Medical Education Online**

This activity has been planned and implemented in accordance with the Essential Areas and policies of the Accreditation Council for Continuing Medical Education through the joint sponsorship of Medscape, LLC and Expert Reviews Ltd. Medscape, LLC is accredited by the ACCME to provide continuing medical education for physicians. Medscape, LLC designates this educational activity for a maximum of 1.0 credit hours **AMA PRA Category 1 Credits™**. Physicians should only claim credit commensurate with the extent of their participation in the activity. All other clinicians completing this activity will be issued a certificate of participation. To participate in this journal CME activity: (1) review the learning objectives and author disclosures; (2) study the education content; (3) take the post-test and/or complete the evaluation at www.medscapecme.com/journal/expertophth; (4) view/print certificate.

Learning objectives

Upon completion of this activity, participants should be able to:

- Describe the characteristics of optical coherence tomography (OCT)
- Describe the disadvantages of scanning Scheimpflug photography in the investigation of glaucoma
- List types of glaucoma for which ultrasound biomicroscopy (UBM) is particularly useful
- Identify cases of glaucoma suitable for OCT or UBM
- Identify the uses of OCT and UBM in glaucoma management

 10.1586/EOP.09.61 ISSN 1746-9899

Financial & competing interests disclosure

Editor

***Elisa Manzotti**, Editorial Director, Future Science Group, London, UK.*

***Disclosure:** Elisa Manzotti has disclosed no relevant financial relationships.*

CME Author

Désirée Lie, MD, MSEd

Clinical Professor, Family Medicine, University of California, Irvine, Orange, CA, USA; Director of Research and Patient Development, Family Medicine, University of California, Irvine, Medical Center, Rossmoor, CA, USA

***Disclosure:** Désirée Lie has disclosed the following relevant financial relationship: she has served as a nonproduct speaker for 'Topics in Health' for Merck Speaker Services.*

Authors and Credentials

Roxana Ursea, MD, MSEd

Assistant Professor of Ophthalmology; Director, Cornea and Refractive Surgery Division, Department of Ophthalmology, University of Arizona, Tucson, AZ, USA

***Disclosure:** Roxana Ursea, MD, has disclosed no relevant financial relationships.*

Ronald H Silverman, PhD

Professor, Department of Ophthalmology, Weill Cornell Medical College, NY, USA

***Disclosure:** Ronald H Silverman, PhD, has disclosed a financial interest in ArcScan, Inc., and has partly been funded by NIH grant EB000238.*

Glaucoma is a disease that is essentially an optic neuropathy. Great strides have been made in the last decade in imaging the retinal nerve fiber layer and the optic nerve using optical coherence tomography (OCT). OCT is a noninvasive technique allowing the visualization and measurement of these structures for the assessment of glaucoma progression [1–5]. While damage to the optic and retinal nerves is responsible for the degradation of vision, in most instances this damage is associated with elevated intraocular pressure (IOP). Elevation of IOP results from an imbalance between the production and drainage of aqueous fluid, specifically, increased outflow resistance. Thus, assessment of the anterior segment plays a major role in the diagnosis and treatment of glaucoma.

The traditional tools for the assessment of the angle and anterior segment are the slit-lamp and gonioscopy, in combination with a Goldmann contact lens and classification using the system introduced by Shaffer [6]. Several newer technologies now exist for imaging of the anterior segment, including scanning Scheimpflug (e.g., Pentacam, Oculus, Inc., Lynnwood, WA, USA), and scanning slit-lamp systems (e.g., Orbscan, Orbtek Inc., Salt Lake City, UT, USA). The Pentacam can provide rapid and reproducible measurements of anterior chamber depth and angle width [7], but is limited to visualization of only the angle approach. Scheimpflug photography also does not display the retroiridal structures or the ciliary body, which are of great interest in glaucoma diagnosis [8]. The scanning peripheral anterior chamber depth analyzer is another optically based system. It has high reproducibility in screening for narrow angles, as with other systems using visible light, but may have difficulty in assessing the bottom of the angle, as can be accomplished by OCT and ultrasound biomicroscopy (UBM) [9]. While these visible light systems are undoubtedly useful, especially for screening for narrow angles, OCT (based on near-infrared light) and UBM systems allow imaging of the full-angle anatomy and, in the case of UBM, visualization of retroiridal structures and the ciliary body. Thus, these technologies provide optimal means for the assessment of the anterior segment in glaucoma.

The development of the ultrasound biomicroscope in the early 1990s introduced high-resolution cross-sectional imaging for assessment of the angle and ciliary body. The more recent development of anterior segment OCT (AS-OCT) further enhanced our ability to visualize the angle and other structures relevant to glaucoma diagnosis and management. In this article, we will review and compare the physics of UBM and OCT systems, and describe their contribution to glaucoma evaluation and management.

Table 1. Comparative properties of anterior segment 840-nm frequency-domain optical coherence tomography and 50 MHz ultrasound biomicroscopy systems.

Characteristic	Frequency-domian optical coherence tomography	Ultrasound biomicroscopy
Axial resolution (μm)	5	30
Lateral resolution (μm)	15	60
Vector/s	26,000	1000
Coupling medium	Air	Fluid or gel
Depth of penetration (mm)	~1	~6
Patient position	Sitting	Supine (or sitting, e.g., Artemis)
Operator requirements	Simple exam	Skilled

Ultrasound principles & technology

In ultrasonic imaging, the transducer emits a short acoustic pulse in response to a voltage transient generated by a pulser. As the pulse propagates through a tissue and encounters anatomic structures differing in acoustic impedance (density × speed of sound) from

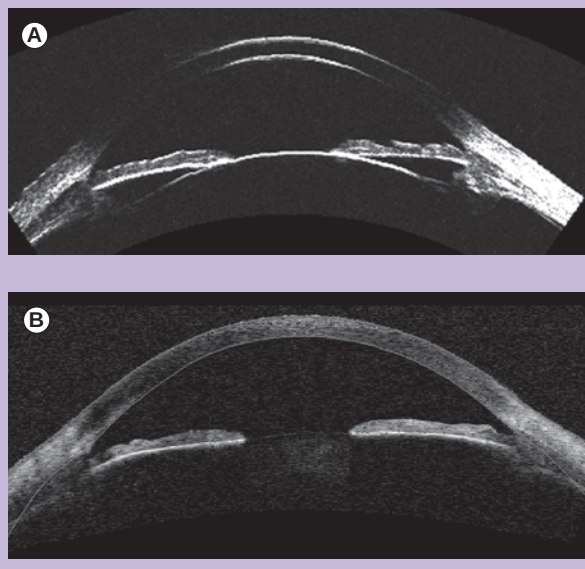

Figure 1. (A) Comparative Artemis – ultrasound biomicroscopy and (B) Visante – optical coherence tomography images of the right eye (undilated) of a 57-year-old male. In both cases, images are in a horizontal plane. There is noticeable bowing forward of the iris and a slight narrowing of the angles in this otherwise normal subject.

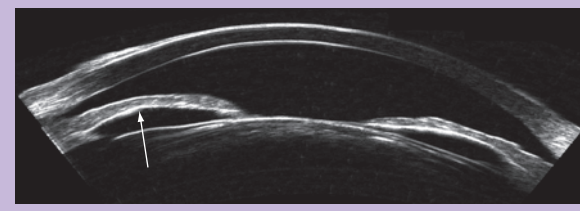

Figure 2. Ultrasound biomicroscopy image of relative pupillary block. The pressure differential between the anterior and posterior chamber causes bowing forward of the iris (arrow) with narrowing of the angles. Peripheral iridotomy will be effective in equalizing pressure between the two chambers.

their surroundings, echoes are generated. When echoes reach the transducer, they are converted back into voltages and amplified. The range of each echo is proportional to the time delay between pulse emission and echo return, specifically, r = ct/2, where r is the range, c is the speed of sound (1532 m/s at 37°C in normal saline) and t is the time. Each pulse/echo event thus provides information along one line of sight. By mechanically scanning the probe, information along an ordered series of lines of sight is obtained. By converting echo amplitude into pixel intensity, a 2D cross-sectional B-scan image is then formed.

Ultrasound resolution improves with increasing center frequency and with bandwidth. Bandwidth describes the range of frequencies present in an ultrasound pulse. As the number of cycles in a pulse increases, bandwidth decreases and resolution degrades. Thus, high resolution demands both high frequency and broad bandwidth.

Ultrasonic imaging of the eye was introduced in the 1950s by Mundt and Hughes (A-scan) [10] and Baum and Greenwood (B-scan) [11], and 10-MHz mechanically scanned ultrasound systems have long since been used for general-purpose imaging of the eye. Such systems are generally designed to be used in contact with the eye or eyelid using a gel or viscous fluid (e.g., methylcellulose), as ultrasound will not otherwise propagate through the air–tissue interface. The 10-MHz ophthalmic B-scanners use a probe whose focus falls on the retina or posterior vitreous. In such a contact B-scanner, the anterior segment is poorly visualized, both owing to the limited resolution (~150 µm at 10 MHz) and because the anterior segment is in the defocused near-field of the probe. While an immersion exam will allow the probe to be offset from the eye sufficiently to place the anterior segment in the focal plane, the limited resolution at 10 MHz reduces diagnostic capacity.

Until the early 1990s, diagnostic ultrasound transducer material was largely limited to lead zirconate titanate crystal. To achieve higher frequencies, the crystal could be made thinner, but above

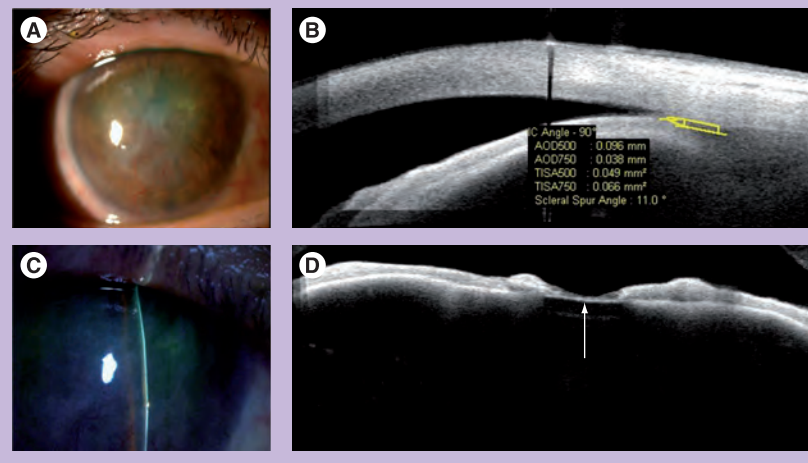

Figure 3. A 52-year-old Hispanic male with neovascular glaucoma and uncontrolled diabetes. (A) Slit-lamp photo shows the slightly hazy cornea, significant superficial and deep neovascularization involving the inferior quadrant and extending to central cornea, and an irregular pupil. **(C)** The oblique slit-beam view shows the shallow anterior chamber. **(B)** The anterior-segment optical coherence tomography confirmed the narrow anterior chamber and enabled good visualization of the very narrow angles (measuring between 11 and 15° in different meridians), the presence of posterior synechiae at the pupillary margin and **(D)** the presence of a dense, thick interpupillary membrane (arrow).

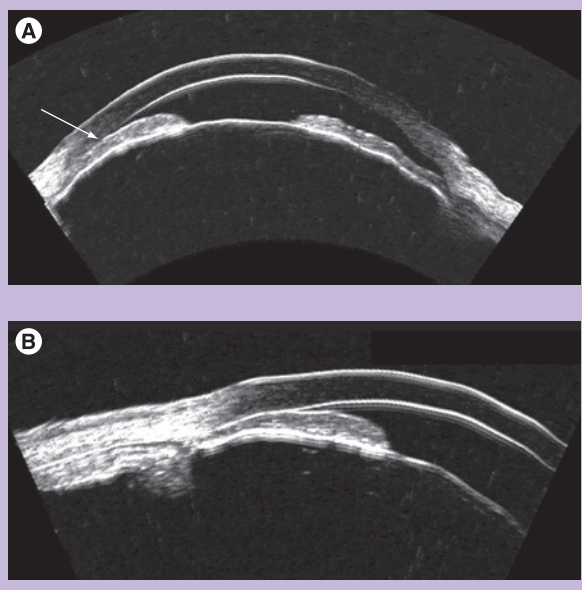

Figure 4. Ultrasound biomicroscopy images of malignant glaucoma. (A) Anterior segment in horizontal plane. **(B)** Temporal quadrant. Note lack of formed posterior chamber, the significant shallowing of the anterior chamber angle and marked iridocorneal touch (arrow). The anterior rotation of the ciliary body at its insertion into the scleral spur may lead to secondary angle-closure glaucoma.

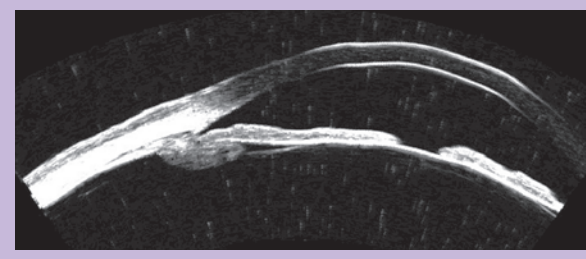

Figure 5. Ultrasound biomicroscopy image of temporal quadrant in patient with plateau iris. Note forward position of ciliary body characteristic for this entity, leading to narrowing of angle by pushing the peripheral iris forward and maintaining its apposition to the trabecular meshwork. The anterior chamber is also shallow.

approximately 15 MHz, this process resulted in unacceptable fragility due to the zirconate titanate's brittleness. By the early 1990s, however, novel polymeric transducer materials (e.g., polyvinylidene fluoride) became available which, for the first time, allowed the production of relatively inexpensive high-frequency transducers [12,13]. Polyvinylidene fluoride membranes could be made sufficiently thin to support frequencies as high as 100 MHz (wavelength: 15 µm) and beyond, and also provided excellent bandwidth. Ultrasound systems utilizing probes of approximately 35 MHz or more have come to be known as UBM or 'very high-frequency ultrasound systems'. Owing to the fact that acoustic attenuation increases exponentially with frequency, such systems are limited to the superficial tissues of the anterior segment.

In the early 1990s, Foster and Pavlin developed the first practical UBM system for imaging of the eye [14,15]. The ultrasound biomicroscope (Zeiss-Humphrey Instruments, San Leandro, CA, USA) was a commercial outgrowth of this work, allowing dissemination of UBM technology and widespread clinical application. Coleman, Silverman and their group at Cornell Medical College (New York, NY, USA) independently developed a UBM system emphasizing the processing of raw radiofrequency echo data acquired in sequential planes suitable for 3D analysis, especially corneal biometric analysis [16]. This system was also eventually commercialized as the Artemis-2 system (Ultralink, LLC, St Petersburg, FL, USA), which uniquely incorporated an optical subsystem for fixation, centration and display of eye position.

The Zeiss-Humphrey (later Paradigm Medical Industries, Salt Lake City, UT, USA) UBM consisted of a 50-MHz probe supported by an articulated arm. The probe provided a scan rate of 8 Hz, giving real-time imaging, with scans consisting of 256 lines of sight (vectors) over a 5 × 5-mm field. This allowed imaging of anatomic areas of

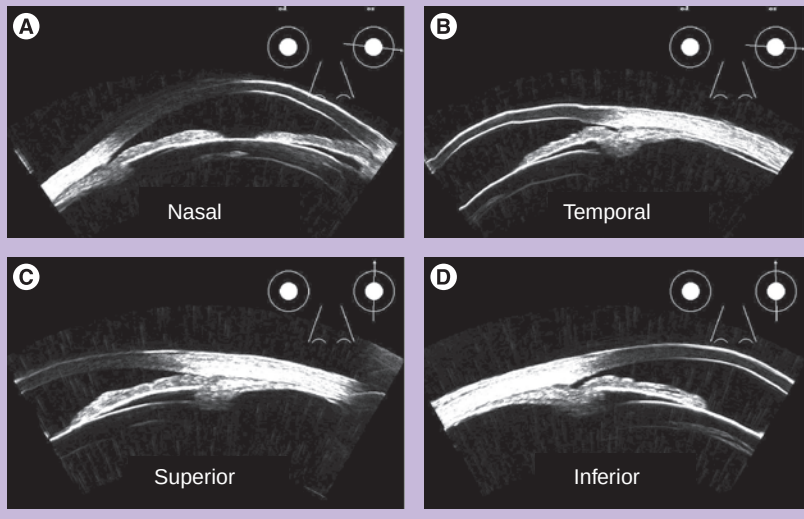

Figure 6. Series of ultrasound biomicroscopy scans covering each quadrant in patient with plateau iris (A–D). Note the shallow anterior chamber and the very narrow angle in all four quadrants. Scans taken before patient underwent a laser peripheral iridotomy followed by an iridoplasty. In plateau iris, the ciliary body is anteriorly placed. The iridotomy addresses the pupillary block component, but not the angle closure related to the abnormal ciliary body position. In such cases, laser iridoplasty is often useful.

interest in the anterior segment, but not the whole anterior segment in a single scan. After topical anesthesia, the probe was coupled to the eye using a plastic scleral shell that held the eyelids open and was filled with normal saline or methylcellulose for acoustic coupling.

Ultrasound biomicroscopy systems are now produced by numerous companies, including Quantel Medical Instruments (Bozeman, MT, USA), Optikon (Rome, Italy), Sonomed (Lake Success, NY, USA) and OPKO (Miami, FL, USA). IScience Interventional (Menlo Park, CA, USA) manufactures an 80-MHz scanner for high-resolution imaging of the angle and Schlemm's canal. Arcscan, Inc. (Golden, CO, USA) is developing a successor to the Artemis-2. Handheld UBM probes are now often equipped with acoustically transparent, fluid-filled 'bubble tips' that can be placed directly onto the globe. These obviate the use of water-baths or scleral shells for acoustic coupling, greatly simplifying the examination and allowing the patient to be examined in a sitting position. In some cases, these instruments provide scan width sufficient to encompass the entire anterior segment, from angle-to-angle and sulcus-to-sulcus in a single image.

OCT principles & technology

Optical coherence tomography of the eye was first described by Huang and coworkers at the Massachusetts Institute of Technology (Boston, MA, USA) in 1991 [17]. OCT is sometimes referred to as an optical analog of ultrasound, but detects optical backscatter instead of acoustic backscatter. 2D OCT images are similarly known as B-scans [18]. As in ultrasound imaging, OCT images are constructed by combining data from multiple closely spaced lines of sight. Optical backscatter results from the presence of refractive index discontinuities, which, in soft tissues, may include connective tissues, cytoplasmic organelles, cell nuclei and melanin granules [19]. However, owing to the fact that the speed of light is so much faster than that of sound, the time delay between the emission of a light pulse and detection of a reflection is too brief to measure directly. Hence, rather than using a pulse–echo technique, a low-coherence light beam (typically a superluminescent diode emitting in the near-infrared region) is split into reference (mirror) and sample (tissue) paths, and then recombined interferometrically. In time-domain OCT, the reference mirror is mechanically scanned in the range axis, and this allows determination of the range to optical reflections along the tissue path, which are represented by interference fringes in the OCT signal.

As with ultrasound, the resolution of OCT is affected by bandwidth and wavelength. OCT imaging, especially of the retina, is also affected by the optical absorption of water, which makes up most of the vitreous. Absorption is low at 820 nm, allowing this wavelength to readily probe the retina. This technique has had a deep impact on the evaluation of the retina, macula and optic nerve by providing real-time images with less than 10-µm resolution.

In the more recently developed frequency (Fourier) domain OCT, the broadband signal is broken into a spectrum using a grating or linear detector array, and depth is determined from the Fourier transform of the spectrum without motion along the reference arm [20]. This allows data along one line of sight to be acquired virtually instantaneously, with the acquisition speed of the photodetector becoming the rate-limiting factor. An alternative implementation involves the use of a frequency-swept light source [21].

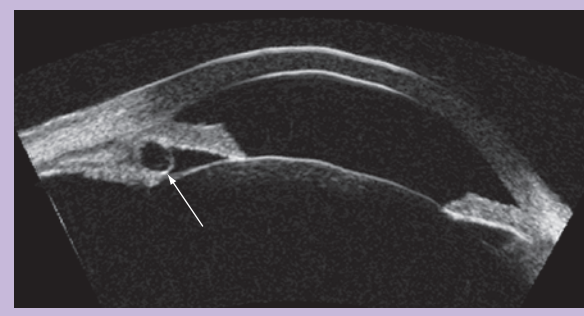

Figure 7. Focal angle closure due to presence of iridociliary cyst (arrow) pushing the iris anteriorly.

The first use of OCT for anterior segment imaging was reported by Izatt and coworkers, who developed a slit-lamp-mounted, 830-nm time-domain device [22]. Spectral domain OCT imaging of the anterior segment at 1310 nm has also been described [23]. Here, the longer wavelength is advantageous in that higher light intensities may be used, improving the signal-to-noise ratio, since most light entering the eye will be absorbed by the vitreous, protecting the retina from damage [24].

The early commercial OCTs introduced by Zeiss utilized the time-domain method for imaging the retina at 820 nm in the near-infrared region. The Visante™ anterior segment OCT system (Carl Zeiss Meditec, Dublin, CA, USA) is also a time-domain device, but operating at 1310 nm. It supports several

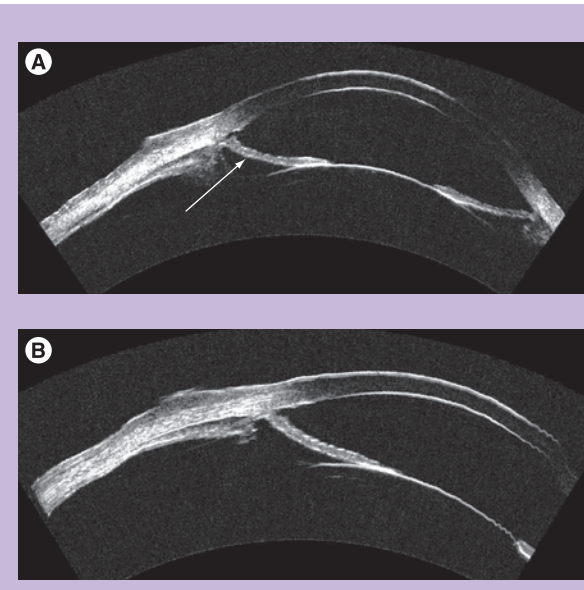

Figure 8. Ultrasound biomicroscopy images of pigmentary glaucoma (A & B). Reverse pupillary block leads to iris concavity (arrow), which can be treated with laser iridotomy.

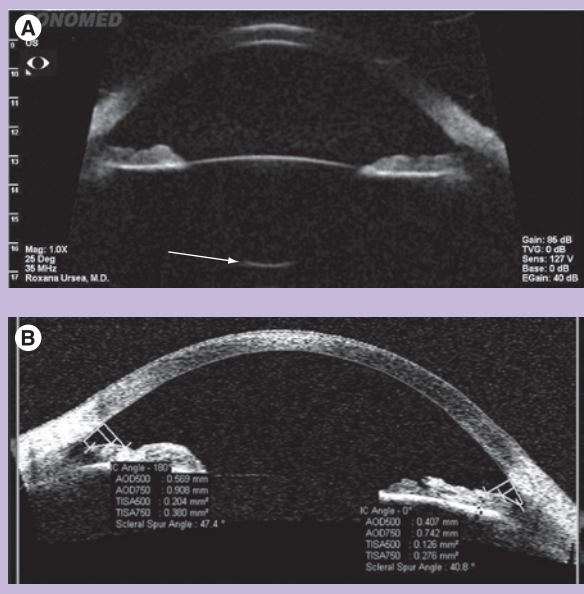

Figure 9. (A) Ultrasound biomicroscopy and (B) optical coherence tomography images in angle-recession glaucoma in horizontal plane of left eye in 45-year-old male patient with history of trauma. Note the deeper penetration with ultrasound biomicroscopy, which allows visualization of the posterior lens capsule centrally (arrow).

modes, including high-resolution cornea, corneal pachymetry and anterior segment. The latter mode consists of 256 vectors, with images acquired in 0.125 s. Resolution is 18 µm axially by 60 µm laterally. The SL-OCT (Heidelberg Engineering, GmbH, Dossenheim, Germany) combines an OCT with a Haag–Streit slit lamp for improved assessment of the iridocorneal angle [25]. The RTVue (Optoview, Inc., Fremont, CA, USA) is a frequency-domain OCT utilizing an 840-nm wavelength. The instrument, originally designed for retinal imaging, utilizes an optional lens for anterior segment imaging. The improved acquisition speed (26,000 vectors/s) and signal-to-noise ratio obtained with frequency-domain processing plus the higher resolution (5 µm axially × 15 µm laterally), obtainable at 840 nm, provides high-quality images of anterior-segment structures. A recent report also describes modification of the Cirrus™ HD-OCT (Carl Zeiss Meditec), a frequency-domain instrument designed for retinal imaging, with a 60-diopter lens, adapting it for imaging of the anterior segment, providing scan rate and resolution comparable to that of the RTVue [26]. The improved resolution of these 840-nm systems allows resolution of structures such as Descemet's membrane, the trabecular meshwork and Schwalbe's line.

Table 1 compares UBM and AS-OCT in terms of resolution and usage. Comparative AS-OCT and UBM images of the anterior segment are presented in Figure 1. In both imaging modes, there is a noticeable bowing forward of the iris plane with slight narrowing of the angles. The UBM image shows greater detail on retroiridal structures, including the ciliary body, zonules and the lens surface. Several recent studies have compared anterior-segment OCT with UBM in detail [27–29]. Garcia and Rosen, using an OTI AS-OCT (Ophthalmic Technologies, Inc., Toronto, ON, Canada) concluded that UBM was advantageous for viewing structures posterior to the iris (whose pigment epithelium strongly absorbs light) and the sclera (which strongly scatters light), and for light–dark studies in glaucoma [27], as previously described by Gazzard *et al.* [30]. Nolan described the advantage of UBM for the detection of cyclodialysis clefts in the ciliary body, and the value of AS-OCT as a noncontact examination technique for rapid follow-up following treatment [28]. Dada *et al.* compared biometric parameters related to the anterior chamber and angle obtained with UBM and OCT, and found them to be comparable [29].

Clinical application of UBM & AS-OCT for glaucoma diagnosis & management

Pavlin and coworkers carried out the first clinical UBM studies of the anterior segment in glaucoma in the early 1990s [31,32]. Pavlin and others demonstrated the utility of UBM in characterizing several forms of glaucoma, including plateau iris syndrome [33] and pupillary block [34], which together constitute the most common forms of primary angle-closure glaucoma [35].

In pupillary block (Figures 2 & 3), pressure in the posterior chamber is elevated relative to that of the anterior chamber owing to impairment of the flow of aqueous through the pupil. This results in forward bowing of the iris from the root to the pupil margin in the presence of a formed posterior chamber. Laser peripheral iridotomy will result in iris flattening by relieving the anterior–posterior chamber pressure differential. UBM has been shown to be of value in elucidating the etiology of pupillary block glaucoma [34,36,37]. UBM can also be useful for the diagnostic imaging of malignant glaucoma (Figure 4), which is characterized by a forward movement of the iris–lens diaphragm and a very shallow

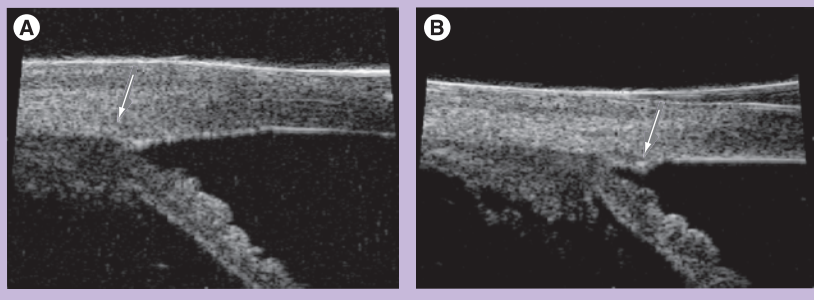

Figure 10. Two 80-MHz ultrasound biomicroscopy images of the angle pre- and 6 months postcanaloplasty. (A) In the pretreatment image, the position of Schlemm's canal is indicated by arrow. **(B)** Post-treatment, Schlemm's canal is widened. Arrow indicates position of suture within canal.
Reprinted with permission from Ian Ugi, Landshut, Germany.

anterior chamber, typically following glaucoma surgery, chronic angle-closure glaucoma or pseudoexfoliation [38]. The primary consideration in the differentiation of pupillary block and malignant glaucoma is the presence of a formed posterior chamber in the former, which can be demonstrated by UBM.

In plateau iris syndrome (Figures 5 & 6), the ciliary body is anteriorly positioned and possibly enlarged, compressing the iridocorneal angle and placing the peripheral iris in apposition to the trabecular meshwork, impairing outflow [33,39]. UBM and OCT will demonstrate little iris bowing, but rather a steep rise in the iris near its point of insertion. Anterior positioning of the ciliary processes and absence of the sulcus are best visualized with UBM. In some cases, multiple ciliary body cysts, also detectable by UBM, can cause a similar effect on the angle (Figure 7) [40–42]. UBM has shown that iridociliary cysts are more common than initially thought, and allows their progression to be followed over time. Although ciliary body cysts are common and generally benign, impaired outflow may result when multiple cysts further narrow an angle that is already compromised by age-related anterior-chamber shallowing [43]. UBM should be performed in all atypical cases of narrow-angle glaucoma. When an iridociliary cyst is detected, management should include UBM examination of both eyes over 360° to rule out any potential angle compromise. Patients with multiple bilateral cysts compromising the angle should be followed as glaucoma suspects. However, if less than 1 clock-hour of angle is narrowed, no follow-up is required.

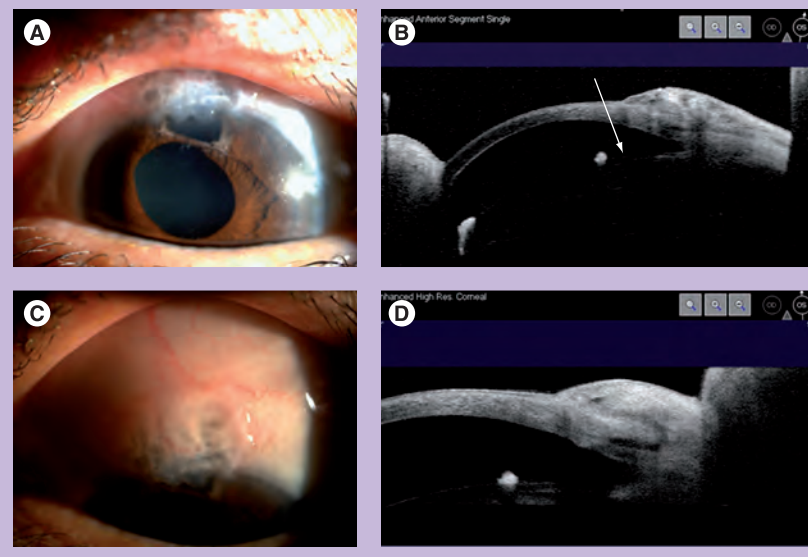

Figure 11. Anterior-segment optical coherence tomography images of filter bleb in 48-year-old Hispanic female with chronic open-angle chronic glaucoma. **(A & C)** Slit-lamp photos in downgaze showing the location of the bulging and translucent bleb, partially covering the superior cornea. **(B & D)** Vertically oriented Visante™ anterior-segment optical coherence tomography images show the large superior surgical peripheral iridotomy (arrow) and the elevation of the bleb. Calipers can be used to measure its height and length.

Sihota and coworkers demonstrated the UBM to be instrumental in characterizing the anatomical features of eyes with primary angle-closure glaucoma: thinner iris, shorter trabecular ciliary process distance and narrow angle [44]. Acute primary angle-closure glaucoma seems to have the narrowest angle recess of all conditions. The major advantage of UBM remains that it provides images of the position, angulation and anatomical variants of the ciliary body and peripheral iris.

Pigment-dispersion glaucoma results from the dissemination of pigment granules from the posterior of the iris as a result of friction between this surface and the zonules and/or lens. The deposition of particles in the trabecular meshwork can impair outflow and lead to an increase in IOP. The UBM appearance of pigment dispersion glaucoma was first described by Pavlin [45]. Pigment dispersion syndrome typically demonstrates an open angle and iris concavity (Figure 8) consistent with the hypothesis that iris–zonular chafing is responsible for the dispersion of pigment particles [46,47]. To account for the concave iris geometry, it has been suggested that a reverse pupillary block is present, as the concavity can often be reversed with iridotomy [48]. Detry-Morel *et al.* described the combined use of OCT and UBM for the diagnostic imaging of pseudophakic secondary pigment dispersion glaucoma, using OCT to demonstrate intermittent iris–intraocular lens contact through a dilated pupil [49]. Yip *et al.* found the Pentacam to be useful for the diagnosis of pigment dispersion glaucoma, reporting that the

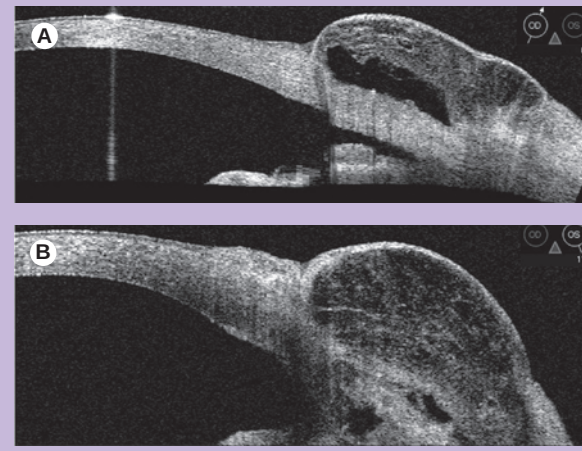

Figure 12. Optical coherence tomography images of filter blebs post-trabeculectomy in the right (A) and left (B) eyes of an 89-year-old male. Note the narrow angle in the right eye scan and the large cystic space within the bleb. The wall of the bleb is nicely delineated and evidenced by the anterior-segment optical coherence tomography.

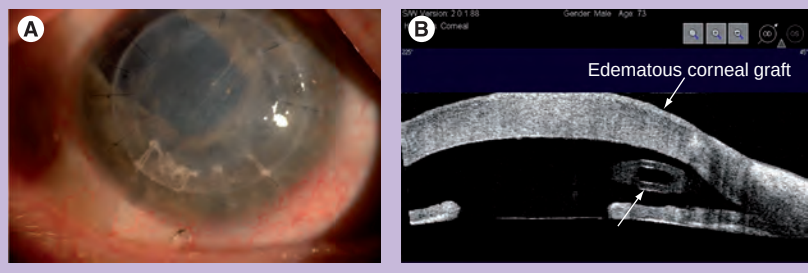

Figure 13. Good positioning with no endothelial touch of a shunt tube (bottom arrow) seen in cross-section with optical coherence tomography in anterior chamber of a 73-year-old patient with hazy cornea postpenetrating keratoplasty. (A) Slit lamp photo showing a corneal graft with Descemet folds, few residual interrupted corneal sutures, a large postsurgical pupil with corectopia and a tube shunt located in the superonasal quadrant. **(B)** Visante™ OCT shows good positioning of shunt tube (large arrow) with no endothelial touch. Note the thickened cornea corresponding to the graft.

posterior cornea exhibited a significantly flatter radius of curvature than in normal eyes, and that this effect increased with pigment loss [50]. He hypothesized that corneal biomechanics may play a role in the etiology of this syndrome.

Choroidal thickening, leading to increased vitreous cavity pressure, has been suggested to be a potential precipitating factor in angle closure [51]. Kumar [52] and Sakai [53] utilized UBM to document the presence of choroidal effusion in patients with primary angle-closure glaucoma and acute angle closure, both pre- and postiridotomy. Gazzard *et al*. were among the first to describe the association of primary acute angle closure with suprachoroidal fluid [54].

Yao *et al.* used UBM under dark conditions to investigate the occurrence of appositional angle closure in postiridotomy fellow eyes of patients with acute-angle closure [55]. Over one third of fellow eyes showed appositional angle closure, indicative of a narrower angle, a more anterior position of the ciliary body and a thicker peripheral iris, suggesting increased risk for progressive angle closure in the fellow eyes.

Angle-recession glaucoma may occur following ocular trauma. Comparative UBM and AS-OCT images in a case of angle recession are shown in Figure 9. Ozdal compared UBM with gonioscopy following such trauma and reported UBM to be diagnostically useful in imaging angle recession, cyclodialysis, zonular deficiency, lens dislocation and synechiae [56]. Kawana *et al.* described the use of a prototype 3D swept-source, 1310-nm OCT to image post-traumatic angle recession [57]. OCT is advantageous in not requiring physical contact with a traumatized eye, but UBM enables the evaluation of the ciliary body, lens and zonules. UBM is a valuable tool in the detection of intraocular foreign bodies affecting the angle or ciliary body after perforating trauma. The noninvasive nature (especially using a bubble-tip set-up) and good penetration of UBM are helpful in the accurate characterization and localization of intraocular foreign bodies, and surgical planing.

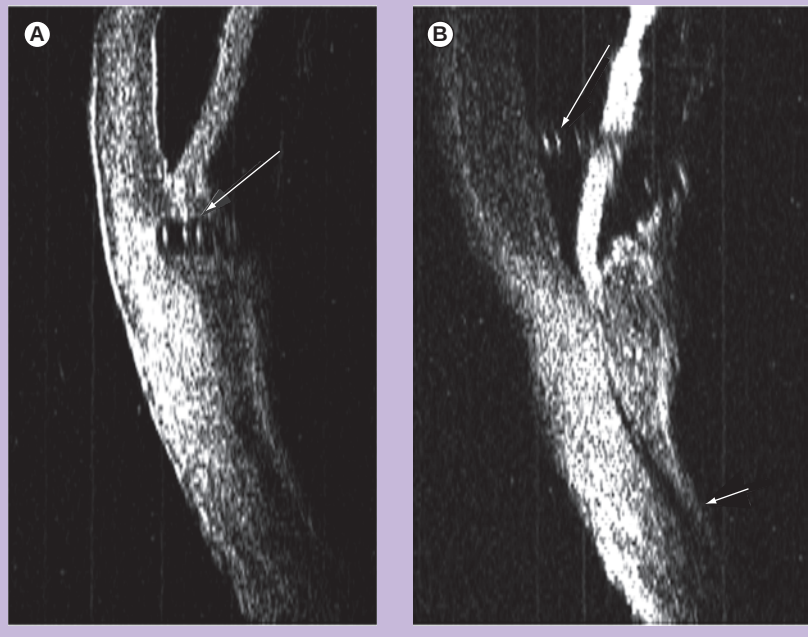

Figure 14. Ultrasound biomicroscopy views of Molteno tube (arrows) before and after entering anterior chamber (A & B). Note acoustic shadow of tube on iris in image on right, and the presence of shallow ciliary body detachment (short arrow).

Ultrasound biomicroscopy and OCT are both useful tools for the planning and guidance of glaucoma surgery [58], including the evaluation of filtering blebs [59,60], sclerectomy [61,62] and canaloplasty [63,64], as well as the diagnosis and evaluation of postoperative complications. Figure 10 shows 80-MHz UBM images of the angle pre- and postcanaloplasty.

Ultrasound biomicroscopy and OCT are superior to slit lamp for the evaluation of bleb function and failure, allowing a demonstration of flattened, encapsulated and cystic avascular thin-walled blebs. In patients with filtering blebs, the AS-OCT can be performed immediately after surgery because nothing touches the eye for scanning. By contrast, the UBM procedure has some risk of bleb wall damage and infection through the eyecups used. The height, wall thickness, apposition of the scleral flap to sclera and the patency of the internal ostium can be assessed. Bleb assessment with UBM or AS-OCT can

Table 2. Biometric parameters used in optical coherence tomography and ultrasound biomicroscopy for characterizing the angle and anterior segment (numerous other parameters beyond this list have been described).

Parameter	Abbreviation	Unit	Description	Ref.
Angle-opening distance	AODn	µm	Distance from cornea to iris at n µm from the scleral spur (n typically 500 or 750)	[31,33]
Trabecular–iris contact length	TICL	µm	Linear distance of contact between iris and cornea/sclera beginning at scleral spur	[55]
Angle-recess area	ARAn	µm^2	Area of triangle between angle recess and iris and cornea n µm from scleral spur (n typically 500 or 750)	[74]
Trabecular–iris space	TISA	µm^2	Area of trapezoid between iris and cornea from sclera to n µm (n typically 500 or 750)	[55]
Trabecular–iris angle	TIA	Degrees	Angle formed from angle recess to points 500 µm from scleral spur on trabecular meshwork and perpendicular on surface of iris	[31,33]
Trabecular–ciliary process distance	TCPD	µm	Measured from point on endothelium 500 µm from scleral spur through iris to ciliary process	[31,33]
Iris–zonular distance	IZD	µm	Distance from posterior iris surface to first visible zonule at point closest to ciliary body	[31,33]
Iris thickness	IT	µm	Measured from perpendicular 500 µm from scleral spur, and possibly other points	[31,33]
Scleral spur–iris insertion distance	SS-IR	µm	Linear distance from scleral spur to iris insertion	[83]
Iris radius of curvature	IRC	mm	Radius of posterior iris surface using an arc transecting three points: iris root, pupil margin and point of maximal iris displacement	[83]
Iris convexity	IC	mm	Maximum distance from the posterior surface of the iris to the line from posterior iris at pupillary margin to the iris root	[78]
Iris–lens contact distance	ILCD	mm	Length of contact between surfaces of lens and iris	[74]
Anterior–posterior chamber depth	ACD/PCD		Ratio of anterior chamber to posterior chamber depth measured 1 mm from the scleral spur	[66]

influence clinical decision-making regarding laser suture lysis following trabeculectomy [65]. AS-OCT images of filter blebs are shown in Figures 11 & 12.

Bochmann *et al.* described the use of UBM for identifying narrow-diameter (<100 µm) iridotomy sites, which were then retreated based on the UBM findings [66]. Ishikawa *et al.* demonstrated that indentation of the cornea by a small eyecup can result in angle widening [67]. Following upon this work, Matsunaga *et al.* described the use of a special UBM eyecup that allowed simultaneous corneal compression with UBM observation of the angle configuration before and after compression [68]. This allowed a differentiation of appositional angle closure from synechial closure. Carillo demonstrated the usefulness of UBM to diagnose obstruction of an Ahmed valve by the iris [69]. UBM may also potentially offer intraoperative guidance in the anterior segment as a supplement to gonioscopy and intraocular microendoscopy [70].

Postpenetrating keratoplasty glaucoma is a major cause of graft failure and the most common cause of irreversible visual loss after keratoplasty. UBM allows imaging of anterior-segment anatomy in the presence of corneal opacity. The visualization of synechiae and secondary angle closure by UBM in such cases can be a valuable tool for planning filtering surgery or the implantation of drainage devices [71].

In glaucoma shunts, the AS-OCT technique allows visualization of the shunt cross-section within the anterior chamber, even, in some instances, in the presence of corneal haze, as demonstrated in Figure 13 in an eye following postpenetrating keratoplasty. By contrast, the UBM is able to evaluate glaucoma tube shunts placed beneath the sclera or iris plane (Figure 14). Rothman *et al.* demonstrated that UBM is instrumental in diagnosing the presence and cause of tube obstruction, as it can detect focal obstructions of Baerveldt tubes caused by kinking at the scleral entry site after pars plana insertion [72].

In 1992, Pavlin described UBM biometric criteria that could be used for reproducible measurement of various anterior segment structures [31]. These included the angle opening at 250 and 500 µm from the scleral spur, scleral thickness at the spur, trabecular–ciliary process distance and iris thickness at specific positions. Tello *et al.* reported on the reproducibility of these measures in 1994 [73]. Ishikawa, Liebman and Ritch described further criteria in 2000, especially numeric descriptors of angle geometry [74]. These criteria are of importance in allowing the definition of reproducible criteria for characterizing different glaucoma types and for documenting change with time or with treatment. Marchini, for instance, used UBM to biometrically

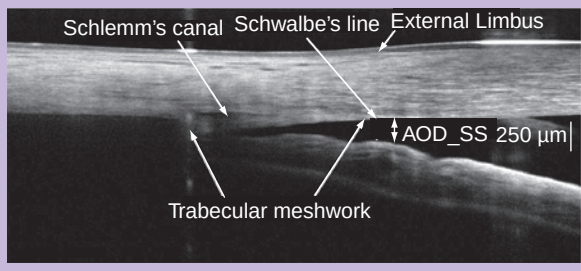

Figure 15. Narrow angle imaged with RTVue Fourier-domain optical coherence tomography with corneal adaptor module.
AOD_SS: Angle-opening distance at Schwalbe's line.
Reprinted with permission from David Huang, MD, PhD and Brian Francis, MD, Doheny Eye Institute, Los Angeles, CA, USA.

compare different forms of angle closure glaucoma [75,76], and Sihota *et al.* applied these criteria for comparing subtypes of primary angle-closure glaucoma [44]. Ramani used UBM to compare anterior-segment biometry between primary angle-closure suspects and age-matched controls, including parameters such as trabecular–ciliary process distance, iris thickness and angle width (in degrees) [77]. Nonaka *et al.* described the use of UBM for the measurement of iris convexity in primary angle-closure glaucoma [78]. Many criteria developed for the assessment of the anterior segment were immediately applicable to AS-OCT when this technology became available. Currently, visualization of the angle in the Visante's high-resolution mode provides clinicians

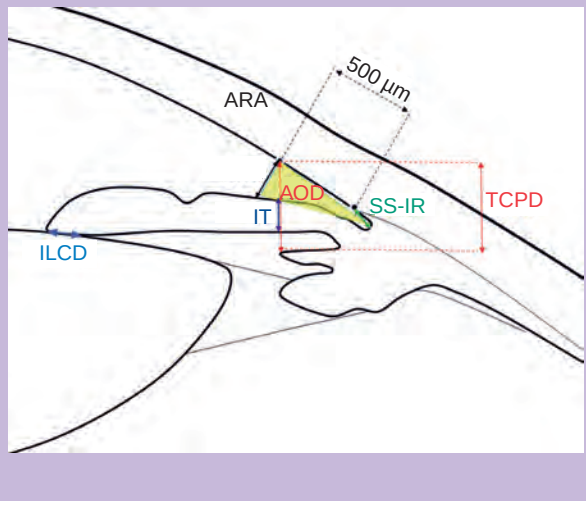

Figure 16. Diagram illustrating several biometric descriptors of the angle, including angle-opening distance, iris thickness, trabecular-ciliary process distance, scleral spur–iris insertion distance and angle recess area. In this example, measurements are made 500 µm from the scleral spur.
AOD: Angle-opening distance; ARA: Angle-recess area; ILCD: Iris–lens contact distance; IT: Iris thickness; SS-IR: Scleral spur–iris insertion distance; TCPD: Trabecular–ciliary process distance.

with optimal anatomical and numerical information on angle anatomy. Frequency-domain OCT provides especially good resolution, enabling the utilization of Schwalbe's line, for instance, as a biometric landmark (Figure 15). A recent comparative UBM and AS-OCT study by Radhakrishnan *et al.* on 31 eyes of normal and narrow-angle subjects found that the anterior-chamber angle parameters measured by both AS-OCT and UBM had similar mean values, reproducibility and sensitivity–specificity profiles [23].

Table 2 describes a variety of biometric parameters that have been developed for OCT and/or UBM for assessment of the angle and anterior segment in glaucoma. Some of these are illustrated in Figure 16.

Numerous clinical studies utilizing OCT and/or UBM have made use of these biometric parameters. Sakata *et al.* compared open-angle subjects with patients with occludable angles on gonioscopy following laser iridotomy [79]. Over half of occludable-angle eyes had appositional angle closure, although this was also found in approximately 20% of normal eyes. A long ciliary process with no ciliary sulcus was observed in 61% of occludable-angle eyes, and also in 32% of control eyes. Gazzard *et al.* described anterior segment morphology changes following laser iridotomy in Asian eyes [80]. Using UBM, Dada *et al.* compared changes in anterior-chamber anatomy in patients with primary angle closure and primary angle-closure glaucoma following iridotomy, demonstrating widening of the anterior-chamber angle and a deepening of the anterior chamber in eyes with primary angle closure, but no significant change in eyes with primary angle-closure glaucoma [81]. Dada also described the UBM changes occurring during a Valsalva maneuver: narrowing of the anterior-chamber angle recess, thickening of the ciliary body and increased iris thickness. In eyes anatomically predisposed to primary angle closure, the Valsalva maneuver may lead to angle closure. The lack of response to iridotomy in primary angle-closure glaucoma is attributed to the closure of the angle by extensive peripheral anterior synechiae (PAS). Yoo *et al.* compared anterior segment biometric parameters in angle-closure suspect eyes with and without PAS [82]. They report that the trabecular–ciliary process distance was significantly shorter in the superior quadrant of PAS eyes when compared with the eyes without PAS, suggesting that the shorter distance from trabecular meshwork to the ciliary body or the anterior placement of ciliary process may play a role in the development of PAS in angle-closure glaucoma suspect eyes. Also studying the effect of iridotomy on angle-closure suspect eyes, He *et al.* found iridotomy to result in a significant increase in angle width, but with some iridotrabecular contact in 59% of eyes with a patent iridotomy [83]. This was associated with smaller angle dimensions and a thicker iris, both of which may play a causative role in maintaining angle closure after iridotomy. Kaushik *et al.* compared UBM and gonioscopy in evaluating changes in angle anatomy following laser iridotomy [84]. They report that the angle significantly widened in the quadrant with iridotomy and the quadrant furthest away in patients of chronic angle closure with established glaucomatous damage. This change was

much better appreciated by UBM than gonioscopy. OCT has also recently been applied for assessment of the angle and iridotomy. In 2005, Chalita *et al.* described the use of a 1300-nm prototype OCT system for the evaluation of a patient with bilateral occludable angle closure pre- and postiridotomy [85]. They demonstrated the iridotomy site as well as an increase in the trabecular–iris area following treatment. More recently, Lei *et al*. used the Visante to study the effects of iridotomy in primary angle closure, concluding that iridotomy leads not only to an increase in peripheral anterior chamber depth and anterior chamber volume, but also to an increase in central anterior-chamber depth [86].

Traditional methods to assess the iridocorneal angle and iris include gonioscopy exam and the van Herick method. Gonioscopy requires a diagnostic contact lens; also, the angle grading is subjective, depending on the good visualization of specific angle structures. The Van Herick technique assesses peripheral anterior chamber depth in relation to corneal thickness. By contrast, both AS-OCT and the UBM provide angle visualization. AS-OCT can be employed as a screening tool for primary angle-closure glaucoma, as it is a noncontact procedure and is less dependent on examiner skills than UBM.

Limitations of the UBM include the requirement of a coupling medium and the patient being scanned in a supine position, which might theoretically lead the iris diaphragm to fall back and change the depth of the anterior chamber and the angle opening. Ishikawa *et al*. demonstrated that inadvertent pressure on the eyecup while scanning can influence the angle configuration [74]. Another limitation is represented by the difficulty in pinpointing the exact location of the UBM scan plane (as there is no fixed reference point for the handheld probe), so the angle region measured is located and referred to as nasal, temporal, superior, inferior and not in exact degrees of an arc (the Artemis system is an exception to this, as all UBM images obtained with this system contain embedded information regarding the orientation of scan planes and position of each vector). Compared with OCT, UBM might be more time consuming and require a skilled operator to obtain high-quality precision images. Nevertheless, these limitations are outweighed by the benefit of UBM for visualizing the ciliary body, zonules and posterior chamber, making it an essential tool in defining the mechanism of closure in angle-closure glaucomas. UBM remains the gold standard in cases of plateau iris configuration and imaging of ciliary processes. Its accuracy and ability to visualize behind a clouded cornea makes it very useful in the preoperative assessment of anterior-segment pathology, contributing to optimal surgical planning. The UBM can be used to perform a darkroom provocative test, which elicits information on whether the angle automatically closes in dark conditions. In plateau iris, UBM typically demonstrates an anteriorly directed ciliary body, no ciliary sulcus, a central flat iris plane and commonly iridocorneal contact. UBM is the superior imaging device for diagnosing cyclodialysis clefts (Figure 17) and anterior suprachoroidal effusions. The clefts are not always visible on gonioscopy, but UBM can confirm the diagnosis and estimate the extent of involvement.

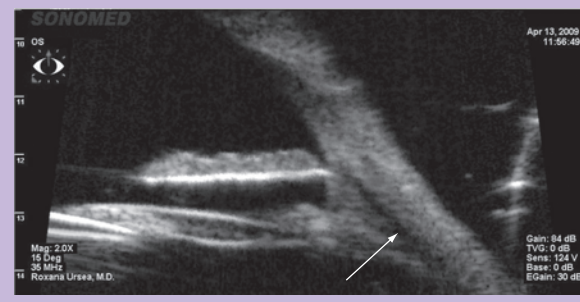

Figure 17. Ciliary body separation (arrow) and cyclodialysis cleft demonstrated by ultrasound biomicroscopy in an 89-year-old pseudophakic veteran. The imaging study was diagnostic and revealed the cause of his long-standing hypotony. Ultrasound biomicroscopy easily assessed the extension of the cleft, which was close to 250° in this patient. In such cases, ultrasound biomicroscopy is superior in diagnosis of the cyclodialysis cleft owing to its ability to penetrate deeper than optical coherence tomography. Optical coherence tomography is limited in its capacity for visualization beyond the iris pigment epithelium. The posterior chamber intraocular lens is partially visualized in this image behind the iris.

Expert commentary

Ultrasound biomicroscopy and OCT can both provide detailed views of anterior segment structures associated with impaired outflow. OCT is advantageous, especially in the case of spectral-domain systems, owing to its superb resolution, high speed and noninvasive character, which allows it to be performed in the immediate postoperative period. UBM is advantageous in that it provides better penetration through opaque or cloudy media than OCT, allowing improved depiction of the ciliary body, retro-iridal structures and the anterior chamber in the presence of corneal edema, scars or hyphema. While neither technique is a substitute

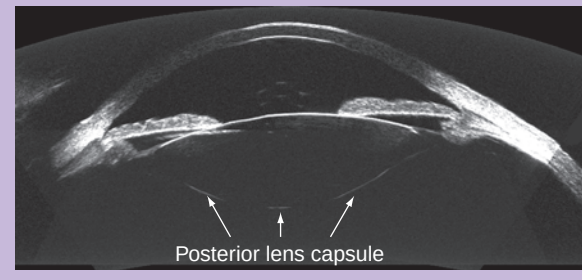

Figure 18. Anterior segment image of normal anterior segment obtained with Artemis-3 prototype. This instrument can utilize a rapid (< 1 s) compound scan mode in which an arc scan is combined with two oblique linear scans to capture the full anterior segment and lens capsule. This technology allows the most accurate angle-to-angle and sulcus-to-sulcus measurements, and may play an important role in lens implant sizing and the preoperative determination of expected lens position.

for gonioscopy, both permit an objective, quantitative description of angle anatomy using a variety of standard biometric parameters for the screening and management of glaucoma.

Five-year view

Several new technologies are being developed for both OCT and UBM. The UBM system being developed by Arcscan, Inc. employs compound scanning for improved depiction of the lens capsule, zonules and other anterior segment structures (Figure 18). High-frequency annular arrays have been developed for improved sensitivity and depth of field [87]. Linear arrays have also been developed, enabling scanning without mechanical motion of the probe [88]. VisualSonics, Inc. (Toronto, ON, Canada) recently introduced a UBM for small animal research with linear arrays of up to 70 MHz providing up to 1000 frames/s. This relative speed increase compared with current single-element mechanically scanned UBM systems is comparable to that of Fourier over time-domain OCT systems. 40-MHz pulsed Doppler has been shown to be applicable to the eye within safe exposure limits [89] and this may offer an avenue for assessing ciliary body perfusion in glaucoma. OCT systems continue to advance in speed, resolution and penetration. This in combination with eye tracking enables the 3D reconstruction of anterior-segment structures [57,60,90]. OCT birefringence imaging of ocular tissues has been introduced [91,92]. This utilizes the alteration of light polarization by fibrous tissue structures to noninvasively detect alterations in such tissues. Yasuno *et al.* recently described the use of 3D polarization-sensitive OCT to assess changes in the anterior segment following glaucoma surgery (trabeculectomy blebs and laser iridotomy sites) [93]. OCT scanning speeds of over 300,000 vectors/s have been achieved [94,95]. These continuing advances in UBM and OCT technology will be translated from the laboratory to commercial instrumentation in the coming years, offering increasing diagnostic capabilities for the assessment of the anterior segment and management of glaucoma.

Acknowledgements

We wish to acknowledge the generous support of Janet and Barry Lang (Roxana Ursea), and that of the Dyson Foundation (Ronald H Silverman).

Key issues

- Both optical coherence tomography (OCT) and ultrasound biomicroscopy (UBM) provide real-time cross-sectional images of the angle and anterior segment.
- Standard biometric descriptors of angle and anterior segment anatomy allow a quantitative approach to glaucoma diagnosis and management.
- OCT advantages versus UBM:
  - Higher resolution
  - Faster scan rate
  - Noncontract method, allowing immediate postoperative use
- UBM advantages versus OCT:
  - Ability to image in the presence of cloudy or opaque media
  - Ability to visualize ciliary body, anterior vitreous, posterior chamber and zonules

References

Papers of special note have been highlighted as:
• of interest

1 Jaffe GJ, Caprioli J. Optical coherence tomography to detect and manage retinal disease and glaucoma. *Am. J. Ophthalmol.* 137, 156–169 (2004).

2 Medeiros FA, Zangwill LM, Bowd C, Vessani RM, Susanna R Jr, Weinreb RN. Evaluation of retinal nerve fiber layer, optic nerve head, and macular thickness measurements for glaucoma detection using optical coherence tomography. *Am. J. Ophthalmol.* 139, 44–55 (2005).

3 Schuman JS, Hee MR, Puliafito CA *et al.* Quantification of nerve fiber layer thickness in normal and glaucomatous eyes using optical coherence tomography. *Arch. Ophthalmol.* 113, 586–596 (1995).

4 Greaney MJ, Hoffman DC, Garway-Heath DF, Nakla M, Coleman AL, Caprioli J. Comparison of optic nerve imaging methods to distinguish normal eyes from those with glaucoma. *Invest. Ophthalmol. Vis. Sci.* 43, 140–145 (2002).

5 Sakata LM, DeLeon-Ortega J, Sakata V, Girkin CA. Optical coherence tomography of the retina and optic nerve – a review. *Clin. Exp. Ophthalmol.* 37, 90–99 (2009).

6 Shaffer RN. A new classification of the glaucomas. *Trans. Am. Ophthalmol. Soc.* 58, 219–225 (1960).

7 Rabsilber TM, Khoramnia R, Auffarth GU. Anterior chamber measurements using Pentacam rotating Scheimpflug camera. *J. Cat. Refr. Surg.* 32, 456–459 (2006).

8 Friedman DS, He M. Anterior chamber angle assessment techniques. *Surv. Ophthalmol.* 53, 250–273 (2008).

9 Kashiwagi K, Kashiwagi F, Toda Y, Osada K, Tsumura T, Tsukahara S. A newly developed peripheral anterior chamber depth analysis system: principle, accuracy, and reproducibility. *Br. J. Ophthalmol.* 88, 1030–1035 (2004).

10 Mundt GH, Hughes WF. Ultrasonics in ocular diagnosis. *Am. J. Ophthalmol.* 42, 488–498 (1956).

11 Baum G, Greenwood I. The application of ultrasonic locating techniques to ophthalmology – part 2. Ultrasonic visualization of soft tissues. *Arch. Ophthalmol.* 60, 263–279 (1958).

12 Sherar MD, Foster FST. The design and fabrication of high frequency poly(vinylide fluoride) transducers. *Ultrason. Imag.* 11, 75–94 (1989).

13 Foster FS, Harasiewicz KA, Sherar MD. A history of medical and biological imaging with polyvinylidene fluoride (PVDF) transducers. *IEEE Trans. Ultrason. Ferro. Freq. Contr.* 47, 1363–1371 (2000).

14 Pavlin CJ, Sherar MD, Foster FS. Subsurface ultrasound microscopic imaging of the intact eye. *Ophthalmology* 97, 244–250 (1990).

15 Pavlin CJ, Harasiewicz K, Sherar MD, Foster FS. Clinical use of ultrasound biomicroscopy. *Ophthalmology* 98, 287–295 (1991).

- **Classic paper describing ultrasound biomicroscopy (UBM) imaging of the eye.**

16 Reinstein DZ, Silverman RH, Coleman DJ. High-frequency ultrasound measurement of the thickness of the corneal epithelium. *Refract. Corn. Surg.* 9, 385–387 (1993).

17 Huang D, Swanson EA, Lin CP *et al.* Optical coherence tomography. *Science* 254, 1178–1181 (1991).

- **Describes optical coherence tomography (OCT) imaging of the retina.**

18 Hee MR, Izatt JA, Swanson EA, Huang D, Schumn JS, Lin CP. Optical coherence tomography of the human retina. *Arch. Ophthalmol.* 113, 325–332 (1995).

19 Tuchin V. Tissue optics. In: *Light Scattering Methods and Instruments for Medical diagnosis (2nd Edition).* SPIE Press, WA, USA (2007).

20 Fercher AF, Hitzenberger CK, Kamp G, El-Zaiat SY. Measurement of intraocular distances by backscattering spectral interferometry. *Optics Comm.* 117, 43–48 (1995).

21 Lee ECW, de Boer JF, Mujat M, Lim H, Yun SH. *In vivo* optical frequency domain imaging of human retina and choroid. *Optics Exp.* 14, 4403–4411 (2006).

22 Izatt JA, Hee MR, Swanson MS *et al.* Micrometer scale resolution imaging of the anterior eye *in vivo* with optical coherence tomography. *Arch. Ophthalmol.* 112, 1584–1589 (1994).

- **Early paper describing anterior-segment OCT.**

23 Radhakrishnan S, Rollins AM, Roth JE *et al.* Real-time optical coherence tomography of the anterior segment at 1310 nm. *Arch. Ophthalmol.* 119, 1179–1185 (2001).

24 Radhakrishnan S, Goldsmith J, Huang D *et al.* Comparison of optical coherence tomography and ultrasound biomicroscopy for detection of narrow anterior chamber angles. *Arch. Ophthalmol.* 123, 1053–1059 (2005).

- **Useful review comparing UBM versus OCT for assessment of the angle.**

25 Wirbelauer C, Karandish A, Haberle H, Pham DT. Noncontact goniometry with optical coherence tomography. *Arch. Ophthalmol.* 123, 179–185 (2005).

26 Wong H-T, Lim CM, Sakata LM *et al.* High-definition optical coherence tomography imaging of the iridocorneal angle of the eye. *Arch. Ophthalmol.* 127, 256–260 (2009).

- **Impressive images of the angle made with high-definition (3–5-µm axial resolution) OCT.**

27 Garcia JP Jr, Rosen RB. Anterior segment imaging: optical coherence tomography versus ultrasound biomicroscopy. *Ophthal. Surg. Laser Imag.* 39, 476–484 (2008).

28 Nolan W. Anterior segment imaging: ultrasound biomicroscopy and anterior segment optical coherence tomography. *Curr. Opin. Ophthalmol.* 19, 115–121 (2008).

29 Dada T, Sihota R, Gadia R, Aggarwal A, Mandal S, Gupta V. Comparison of anterior segment optical coherence tomography and ultrasound biomicroscopy for assessment of the anterior segment. *J. Cat. Ref. Surg.* 33, 837–840 (2007).

30 Gazzard G, Foster PJ, Friedman DS, Khaw PT, Seah SKL. Light to dark physiological variation in irido–trabecular angle width. *Br. J. Ophthalmol.* 88, 1357–1482 (2004).

31 Pavlin CJ, Harasiewicz K, Foster FS. Ultrasound biomicroscopy of anterior segment structures in normal and glaucomatous eyes. *Am. J. Ophthalmol.* 113, 381–389 (1992).

- **Describes what has become the standard biometric parameter set for characterization of the angle.**

32 Pavlin CJ, Foster FS. Ultrasound biomicroscopy in glaucoma. *Acta Ophthalmologica* 204(Suppl.), 7–9 (1992).

33 Pavlin CJ, Ritch R, Foster FS. Ultrasound biomicroscopy in plateau iris syndrome. *Am. J. Ophthalmol.* 113, 390–395 (1992).

34 Aslanides IM, Libre PE, Silverman RH *et al.* High frequency ultrasound imaging in pupillary block glaucoma. *Br. J. Ophthalmol.* 79, 972–976 (1995).

35 Mandell MA, Pavlin CJ, Weisbrod DJ, Simpson ER. Anterior chamber depth in plateau iris syndrome and pupillary block as measured by ultrasound biomicroscopy. *Am. J. Ophthalmol.* 136, 900–903 (2003).

36 Satish S, MacKinnon JR, Atta HR. Role of ultrasound biomicroscopy in managing pseudophakic pupillary block glaucoma. *J. Cat. Refr. Surg.* 26, 1836–1838 (2000).

37 Kobayashi H, Hirose M, Kobayashi K. Ultrasound biomicroscopic analysis of pseudophakic pupillary block glaucoma induced by Soemmering's ring. *Br. J. Ophthalmol.* 84, 1142–1146 (2000).

38 Trope GE, Pavlin CJ, Bau A *et al.* Malignant glaucoma. Clinical ultrasound biomicroscopic features. *Ophthalmology* 101, 1030–1035 (1994).

39 Kumar RS, Baskaran M, Chew PTK *et al.* Prevalence of plateau iris in primary angle closure suspects. *Ophthalmology* 115, 430–434 (2008).

40 Tanihara H, Akita J, Honjo M, Honda Y. Angle closure caused by multiple, bilateral iridociliary cysts. *Acta Ophthalmol. Scand.* 75, 216–217 (1997).

41 Kuchenbecker J, Motschmann M, Schmitz K, Behrens-Baumann W. Laser iridocystotomy for bilateral acute-angle closure glaucoma secondary to iris cysts. *Am. J. Ophthalmol.* 129, 391–393 (2000).

42 McWhae JA, Rinke M, Crichton AC, Van Wyngaarden C. Multiple bilateral iridociliary cysts: ultrasound biomicroscopy and clinical characteristics. *Can. J. Ophthalmol.* 42, 268–271 (2007).

43 Katsimpris JM, Petropoulos IK, Sunaric-Mégevand G. Ultrasound biomicroscopy evaluation of angle closure in a patient with multiple and bilateral iridociliary cysts. *Klin. Monatsbl. Augenheilkd.* 224, 324–327 (2007).

44 Sihota R, Dada T, Gupta R, Lakshminarayan P, Pandey RM. Ultrasound biomicroscopy in the subtypes of primary angle-closure glaucoma. *J. Glaucoma* 14, 387–391 (2005).

- **Very useful paper describing comparative differences in UBM-determined biometric parameters between normal eyes, open-angle glaucoma (subacute and acute) and chronic primary angle-closure glaucoma.**

45 Pavlin CJ, Macken P, Trope GE *et al.* Accommodation and iridotomy in the pigment dispersion syndrome. *Ophthalmic Surg. Lasers* 27, 113–120 (1996).

46 Potash SD, Tello C, Liebmann J, Ritch R. Ultrasound biomicroscopy in pigment dispersion syndrome. *Ophthalmology* 101, 332–339 (1994).

47 Kanadani FN, Dorziraj S, Langlich AM *et al*. Ultrasound biomicroscopy in asymmetric pigment dispersion syndrome and pigmentary glaucoma. *Arch. Ophthalmol*. 124, 1573–1576 (2006).

48 Karickhoff JR. Pigment dispersion syndrome and pigmentary glaucoma: a new mechanism concept, a new treatment, and a new technique. *Ophthalmic Surg.* 23, 269–277 (1992).

49 Detry-Morel ML, van Acker E, Pourjavan S, Levi N, De Potter P. Anterior segment imaging using optical coherence tomography and ultrasound biomicroscopy in secondary pigmentary glaucoma associated with in-the-bag intraocular lens. *J. Cataract Refract. Surg.* 32, 1866–1869 (2007).

50 Yip LW, Sothornwit N, Berkowitz J, Mikelberg FS. A comparison of intraocular differences in patients with pigment dispersion syndrome. *J. Glaucoma* 18, 1–5 (2009).

51 Quigley HA, Friedman DS, Congdon NG. Possible mechanisms of primary angle closure and malignant glaucoma. *J. Glaucoma* 12, 167–180 (2003).

52 Kumar RS, Quck D, Lee KY *et al*. Confirmation of the presence of uveal effusion in Asian eyes with primary angle-closure glaucoma. *Arch. Ophthalmol*. 126, 1647–1651 (2008).

53 Sakai H, Morine-Shinjyo S, Shinzato M, Nakamura Y, Sakai M, Sawaguchi S. Uveal effusion in primary angle-closure glaucoma. *Ophthalmology* 112, 413–419 (2005).

54 Gazzard G, Friedman DS, Devereux J, Seah S. Primary acute-angle closure glaucoma is associated with supra-choroidal fluid in Chinese patients. *Eye* 15(Pt 3), 358–360 (2001).

55 Yao B, Wu L, Zhang C, Wang X. Ultrasound biomicroscopic features associated with angle closure in fellow eyes of acute primary angle closure after laser iridotomy. *Ophthalmology* 116, 444–448 (2009).

56 Özdal MPC, Mansour M, Deschênes J. Ultrasound biomicroscopic evaluation of the traumatized eyes. *Eye* 17, 467–472 (2003).

57 Kawana K, Yasuno Y, Yatagai T, Oshika T. High-speed, swept-source optical coherence tomography: a 3D view of anterior chamber angle recession. *Acta Ophthalmol. Scand*. 85, 684–685 (2007).

58 Yamamoto T, Sakuma T, Kitakawa Y. An ultrasound biomicroscopic study of filtering blebs after mitomycin C trabeculectomy. *Ophthalmology* 102, 1770–1776 (1995).

59 Zhang Y, Wu Q, Zhang M, Song BW, Du XH, Lu B. Evaluating subconjunctival bleb function after trabeculectomy using slit-lamp optical coherence tomography and ultrasound biomicroscopy. *Chin. Med. J.* 121, 1274–1279 (2008).

60 Kawana K, Kiuchi T, Yasuno Y, Oshika T. Evaluation of trabeculectomy blebs using 3D cornea and anterior segment optical coherence tomography. *Ophthalmology* 116, 848–855 (2009).

- **Impressive application of 3D OCT for visualization of bleb internal structure.**

61 Aptel E, Dumas S, Denis P. Ultrasound biomicroscopy and optical coherence tomography imaging of filtering blebs after deep sclerotomy with new collagen implant. *Eur. J. Ophthalmol.* 19, 223–230 (2009).

62 Khairy HA, Atta HR, Green FD *et al*. Ultrasound biomicroscopy in deep sclerotomy. *Eye* 19, 555–560 (2005).

63 Lewis RA, von Wolff K, Tetz M *et al*. Canaloplasty: circumferential viscodilation and tensioning of Schlemm's canal using a flexible microcatheter for the treatment of open-angle glaucoma in adults: interim clinical study analysis. *J. Cataract Refract. Surg.* 33, 1217–1226 (2007).

64 Shingleton B, Tetz M, Korber N. Circumferential viscodilation and tensioning of Schlemm canal (canaloplasty) with temporal clear corneal phacoemulsification cataract surgery for open-angle glaucoma and visually significant cataract. One-year results. *J. Cataract Refract. Surg.* 34, 433–440 (2008).

65 Singh M, Aung T, Aquino MC, Chew PT. Utility of bleb imaging with anterior segment optical coherence tomography in clinical decision-making after trabeculectomy. *J. Glaucoma* 18, 492–495 (2009).

66 Bochmann F, Johnson Z, Atta HR, Azuara-Blanco A. Increasing the size of a small peripheral iridotomy widens the anterior chamber angle: an ultrasound biomicroscopic study. *Klin. Monatsbl. Augenheilkd.* 225, 349–352 (2008).

67 Ishikawa H, Inazumi K, Liebmann JM, Ritch R. Inadvertent corneal indentation can cause artifactitious widening of the iridocorneal angle on ultrasound biomicroscopy. *Ophthalmic Surg. Laser* 31, 342–345 (2000).

68 Matsunaga K, Ito K, Esaki K *et al*. Evaluation and comparison of indentation ultrasound biomicroscopy gonioscopy in relative pupillary block, peripheral anterior synechia, and plateau iris configuration. *J. Glaucoma* 13, 516–519 (2004).

69 Carrillo MM, Trope GE, Pavlin C, Buys YM. Use of ultrasound biomicroscopy to diagnose Ahmed valve obstruction by iris. *Can. J. Ophthalmol*. 40, 499–501 (2005).

70 Dietlein TS, Engels BF, Jacobi PC *et al*. UBM-guided chamber angle surgery for glaucoma management: an experimental study. *Eye* 17, 340–345 (2003).

71 Dada T, Aggarwal A, Vanathi M *et al*. Ultrasound biomicroscopy in opaque grafts with post-penetrating keratoplasty glaucoma. *Cornea* 27, 402–405 (2008).

72 Rothman RF, Sidoti PA, Gentile RC *et al*. Glaucoma drainage tube kink after pars plana insertion. *Am. J. Ophthalmol*. 132, 413–414 (2001).

73 Tello C, Liebmann JM, Potash SD *et al*. Measurement of ultrasound biomicroscopy images: intraobserver and interobserver reliability. *Invest. Ophthalmol. Vis. Sci.* 35, 3549–3552 (1994).

74 Ishikawa H, Liebmann JM, Ritch R. Quantitative assessment of the anterior segment using ultrasound biomicroscopy. *Curr. Opin. Ophthalmol.* 11, 133–139 (2000).

- **Excellent review of anterior segment biometry methods.**

75 Marchini G. Biometric data and pathogenesis of angle closure glaucoma. *Acta Orthop. Scand.* 80(S236), 13–14 (2002).

76 Marchini G, Pagliarusco A, Toscano A *et al*. Ultrasound biomicroscopic and conventional ultrasonographic study of ocular dimensions in primary angle-closure glaucoma. *Ophthalmology* 105, 2091–2098 (1998).

77 Ramani KK, Mani B, Ronnie G, Joseph R, Lingam V. Gender variation in ocular biometry and ultrasound biomicroscopy of primary angle closure suspects and normal eyes. *J. Glaucoma* 16, 122–128 (2007).

78 Nonaka A, Iwawaki T, Kikuchi M, Fujihara M, Nishida A, Kurimoto Y. Quantitative evaluation of iris convexity in primary angle closure. *Am. J. Ophthalmol*. 143, 695–697 (2007).

79 Sakata LM, Sakata K, Susanna R Jr *et al*. Long ciliary processes with no ciliary sulcus and appositional angle closure assessed by ultrasound biomicroscopy. *J. Glaucoma* 15, 371–379 (2006).

80 Gazzard G, Friedman DS, Devereux JG, Chew P, Seah SK. A prospective ultrasound biomicroscopy evaluation of changes in anterior segment morphology after laser iridotomy in Asian eyes. *Ophthalmology* 110, 630–638 (2003).

81 Dada T, Mohan S, Sihota R, Gupta R, Gupta V, Pandey RM. Comparison of ultrasound biomicroscopic parameters after laser iridotomy in eyes with primary angle closure and primary angle-closure glaucoma. *Eye* 21, 956–961 (2007).

82 Yoo C, Oh JH, Jung HR. Peripheral anterior synechiae and ultrasound biomicroscopic parameters in angle-closure glaucoma suspects. *Korean J. Ophthalmol.* 21, 106–110 (2007).

83 He M, Friedman DS, Ge J *et al*. Laser peripheral iridotomy in eyes with narrow drainage angles: ultrasound biomicroscopy outcomes. The Liwan Eye Study. *Ophthalmology* 114, 1513–1519 (2007).

84 Kaushik S, Sumar S, Jain R, Bansal R, Pandav SS, Gupta A. Ultrasound biomicroscopic quantification of the change in anterior chamber angle following laser peripheral iridotomy in early chronic primary angle-closure glaucoma. *Eye* 21, 735–741 (2007).

85 Chalita MR, Li Y, Smith S *et al*. High-speed optical coherence tomography of laser iridotomy. *Am. J. Ophthalmol.* 140, 1133–1136 (2005).

86 Lei K, Wang N, Wang L, Wang B. Morphological changes of the anterior segment after laser peripheral iridotomy in primary angle closure. *Eye* 23, 345–350 (2009).

87 Silverman RH, Ketterling JA, Coleman DJ. High-frequency ultrasonic imaging of the anterior segment using an annular array transducer. *Ophthalmology* 114, 816–822 (2007).

88 Hu CH, Xu XC, Cannata JM *et al*. Development of a real-time, high-frequency ultrasound digital beamformer for high-frequency linear array transducers. *IEEE Trans. Ultrason. Ferroelectr. Freq. Contr*ol 53, 317–323 (2006).

89 Cucevic V, Brown AS, Foster FS. Thermal assessment of 40-MHz pulsed Doppler ultrasound in human eye. *Ultrasound Med. Biol.* 31, 565–573 (2005).

90 Yasuno Y, Madjarova VD, Makita S *et al*. 3D and high-speed swept-source optical coherence tomography for *in vivo* investigation of human anterior eye segments. *Opt. Express* 13, 10652–10664 (2005).

91 Pircher M, Gotzinger E, Findl O *et al*. Human macula investigated *in vivo* with polarization-sensitive optical coherence tomography. *Invest. Ophthalmol. Vis. Sci.* 47, 5487–5494 (2006).

92 Hitzenberger CK, Gotzinger E, Pircher M. Birefringence properties of the human cornea measured with polarization sensitive optical coherence tomography. *Bull. Soc. Belge Ophtalmol*. 302, 153–168 (2006).

93 Yasuno Y, Yamanari M, Kawana K, Oshika T, Miura M. Investigation of post-glaucoma-surgery structures by 3D and polarization sensitive anterior eye segment optical coherence tomography. *Opt. Express* 16, 3980–3996 (2009).

94 Huber R, Wojtkowski M, Fujimoto JG. Fourier domain mode locking (FDML): a new laser operating regime and applications for optical coherence tomography. *Opt. Express* 14, 3225–3237 (2006).

95 Potsaid B, Gorczynska I, Srinivasan VJ *et al*. Ultrahigh speed spectral/Fourier domain OCT ophthalmic imaging at 70,000 to 312,500 axial scans per second. *Opt. Express* 16, 15149–15169 (2008).

Affiliations

- Roxana Ursea, MD
  Assistant Professor of Ophthalmology, Director, Cornea and Refractive Surgery Division, Department of Ophthalmology, University of Arizona, 655 N. Alvernon Way, Suite 108, Tucson, AZ 85711, USA
  Tel.: +1 520 322 3800 ext. 204
  Fax: +1 520 321 3665
  rursea@eyes.arizona.edu
- Ronald H Silverman, PhD
  Professor, Department of Ophthalmology, Weill Cornell Medical College, 1300 York Ave, Room LC303, NY 10065, USA
  Tel.: +1 212 746 6106
  Fax: +1 212 746 8101
  ros2012@med.cornell.edu
  and
  FL Lizzi Center for Biomedical Engineering, Riverside Research Institute, 156 William Street, 9th floor, NY 10038, USA
  Tel.: +1 212 502 1748
  Fax: +1 212 502 1729
  rsilverman@rri-usa.org

MedscapeCME™ Anterior-segment imaging for assessment of glaucoma

To obtain credit, you should first read the journal article. After reading the article, you should be able to answer the following, related, multiple-choice questions. To complete the questions and earn continuing medical education (CME) credit, please go to http://cme.medscape.com/CME/expertreviews. Credit cannot be obtained for tests completed on paper, although you may use the worksheet below to keep a record of your answers. You must be a registered user on Medscape.com. If you are not registered on Medscape.com, please click on the New Users: Free Registration link on the left hand side of the website to register. Only one answer is correct for each question. Once you successfully answer all post-test questions you will be able to view and/or print your certificate. For questions regarding the content of this activity, contact the accredited provider, CME@medscape.net. For technical assistance, contact CME@webmd.net. American Medical Association's Physician's Recognition Award (AMA PRA) credits are accepted in the US as evidence of participation in CME activities. For further information on this award, please refer to http://www.ama-assn.org/ama/pub/category/2922.html. The AMA has determined that physicians not licensed in the US who participate in this CME activity are eligible for AMA PRA Category 1 Credits™. Through agreements that the AMA has made with agencies in some countries, AMA PRA credit is acceptable as evidence of participation in CME activities. If you are not licensed in the US and want to obtain an AMA PRA CME credit, please complete the questions online, print the certificate and present it to your national medical association.

Activity Evaluation
Where 1 is strongly disagree and 5 is strongly agree

	1	2	3	4	5
1. The activity supported the learning objectives.					
2. The material was organized clearly for learning to occur.					
3. The content learned from this activity will impact my practice.					
4. The activity was presented objectively and free of commercial bias.					

1. Which of the following is least likely to be a characteristic of optical coherence tomography (OCT)?
   - ☐ **A** Invasive
   - ☐ **B** Assesses glaucoma progression
   - ☐ **C** Diagnostic for glaucoma
   - ☐ **D** Based on near-infrared light
2. Which of the following is most likely to be a disadvantage of scanning Scheimpflug photography in the investigation of glaucoma?
   - ☐ **A** Visualizes only the angle
   - ☐ **B** Slow in measurement of chamber depth
   - ☐ **C** Does not display ciliary body
   - ☐ **D** Invasive
3. Ultrasound biomicroscopy (UBM) is likely to be useful in the assessment of which of the following subtypes of glaucoma?
   - ☐ **A** Pupillary block glaucoma
   - ☐ **B** Malignant glaucoma
   - ☐ **C** Plateau iris syndrome
   - ☐ **D** All of the above
4. In a patient requiring preoperative planning and assessment of the anterior segment with a cloudy cornea, which of the following methods is most appropriate?
   - ☐ **A** OCT
   - ☐ **B** UBM
   - ☐ **C** Scanning Scheimpflug method
   - ☐ **D** Van Herick method
5. Which of the following is least accurate in describing the OCT and UBM approaches to anterior segment evaluation in glaucoma?
   - ☐ **A** They can substitute for gonioscopy
   - ☐ **B** They provide quantitative measurements of the angle
   - ☐ **C** They are useful for preoperative and postoperative assessment
   - ☐ **D** They allow visualization of the ciliary body